Q. J. R. Meteorol. Soc. (1997), **123**, pp. 1749–1762

A finite-volume integration method for computing pressure gradient force in general vertical coordinates

By SHIAN-JIANN LIN*
University of Maryland, USA

(Received 29 July 1996; revised 10 December 1996)

SUMMARY

A finite-volume integration method is proposed for computing the pressure gradient force in general vertical coordinates. It is based on fundamental physical principles in the discrete physical space, rather than on the common approach of transforming analytically the pressure gradient terms in differential form from the vertical physical (i.e., height or pressure) coordinate to one following the bottom topography. The finite-volume discretization is compact, involving only the four vertices of the finite volume. The accuracy of the method is evaluated statically in a two-dimensional environment and dynamically in three-dimensional dynamical cores for general circulation models. The errors generated by the proposed method are demonstrated to be very low in these tests.

KEYWORDS: Finite-volume discretization Numerical techniques Orography

1. INTRODUCTION

One of the remaining outstanding problems in modelling geophysical flows is the accurate representation of the lower boundary. A continuous topography is implied in terrain-following coordinates. The well-known drawback to the terrain-following approach is that the pressure gradient term becomes two large terms with opposite sign near steep mountains, which usually results in large errors in the numerical representation of the net pressure force. To get around this difficulty, Mesinger (1984) developed the step-mountain approach of the η-coordinate system. Although the difficulty in computing the pressure gradient force is removed, the piecewise constant representation of the terrain should be regarded as only first-order accurate whereas the continuous representation of the terrain in the terrain-following coordinates is at least second-order accurate (depending on the chosen method of discretization). Furthermore, physical parametrizations in the planetary boundary-layer are more straightforward with the terrain-following coordinates. Based on this line of reasoning, the terrain-following coordinate approach should be preferred, particularly at low resolutions, provided that the errors in computing the pressure gradient force can be greatly reduced.

Based on direct coordinate transformation (Phillips 1957; Kasahara 1974), numerous methods have been developed in the past for the pressure-based terrain-following coordinates (e.g., Corby *et al.* 1972; Simmons and Burridge 1981; Arakawa and Suarez 1983; Arakawa and Konor 1996). These methods are generally designed to maintain some integral constraints (such as the energy conservation) of the continuous equations and/or to eliminate the aforementioned errors for some particular thermodynamic profiles. The Simmons–Burridge and the Arakawa–Suarez methods have been widely adopted in atmospheric general circulation models. Another approach is the vertical interpolation of the geopotential from σ back to pressure surfaces (e.g., Smagorinsky *et al.* 1967; Kurihara 1968; Mihailovic and Janjic 1986).

The problem with the coordinate transformation or the interpolation methods is that physical principles as fundamental as Newton's second and third laws are often violated in the discrete physical space. This is due to the inconsistency arising from the use of the continuous hydrostatic relationship in differential form for the coordinate transformation while the discretization of the hydrostatic relationship and the two terms representing

* Corresponding address: NASA Goddard Space Flight Center, Code 910.3, Greenbelt, MD 20771, USA. e-mail: lin@dao.gsfc.nasa.gov.

the pressure gradient force are only discrete approximations. The enforcement of certain integral constraints like those in the Arakawa–Suarez method should help in reducing the inconsistency. However, it is argued that obeying the most basic laws of physics in the discrete space is more important than satisfying the global integral constraints.

It is recalled that dynamical equations governing fluid motions, namely, the Navier–Stokes equations and their derivatives, which include the hydrostatic primitive equations for the atmosphere, are originally derived from the finite (or 'control')-volume approach. It is by assuming that the time and space increments are infinitesimal that the continuous form of the equations is obtained. Inconsistencies with the underlying physics may arise when the continuous equations are later discretized using mathematically derived numerical methods (e.g., Taylor series expansions). It is likely that by not discretizing directly the continuous equations in differential form, wherever possible, more accurate discrete representation of the physics can be obtained. This is the main motivation for deriving the proposed method based on the fundamental laws of the physics for the finite volume.

Stelling and Kester (1994) presented a finite-volume method for the approximation of pressure gradients and the horizontal diffusive fluxes in sigma-coordinates. The Leibnitz rule was utilized for the analytic transformation of the pressure gradients. An auxiliary Cartesian grid is required for the computation of the horizontal fluxes, which increases the algorithm complexity. Their method seems to work best when there is significant physical diffusion in the horizontal direction.

A physically motivated and much simpler finite-volume integration method based directly on the basic laws of the physics is developed in section 2 for height-based terrain-following coordinates (e.g., Gal-Chen and Somerville 1975). Using a direct finite-volume integration of the continuous equation in differential form, an equivalent algorithm for pressure-based coordinates is derived in section 3. These algorithms can in fact be applied to any vertical coordinate (pure sigma, hybrid sigma–P, or hybrid coordinate with a smooth transition to isentropic surfaces). In section 4 the method is evaluated in a two-dimensional (2D) environment with an idealized mountain and in three-dimensional (3D) dynamical cores for general circulation models with realistic topography. It is demonstrated that errors associated with the use of the sigma-coordinate can be greatly reduced as compared to the widely adopted Arakawa–Suarez method (1983). Concluding remarks are given in section 5.

2. The finite-volume discretization in height-based terrain-following coordinates

We shall derive the method in a 2D x–z plane (Fig. 1). The exact form of the vertical coordinate need not be specified. The resultant (vector) pressure force $\Sigma\mathbf{F}$ acting on the finite volume (the shaded region in Fig. 1) is computed as follows:

$$\Sigma\mathbf{F} = \int_C P\mathbf{n}\,\mathrm{d}s \tag{1}$$

where P is the pressure, $\mathbf{n}$ is the normal unit vector pointing inward, and $\mathrm{d}s$ is an element of the contour. The contour integral is taken counter-clockwise along the peripheral of the volume element. Considering only pressure forces, from Newton's second law of motion we have

$$\left(\frac{\mathrm{d}u}{\mathrm{d}t}, \frac{\mathrm{d}w}{\mathrm{d}t}\right) = \frac{1}{\Delta m}(\Sigma\mathbf{F}_x, \Sigma\mathbf{F}_z) \tag{2}$$

where Δm is the mass of the finite volume and $\Sigma\mathbf{F}_x$ and $\Sigma\mathbf{F}_z$ are the horizontal and vertical components of the resultant force, respectively. Other notations are standard. Newton's

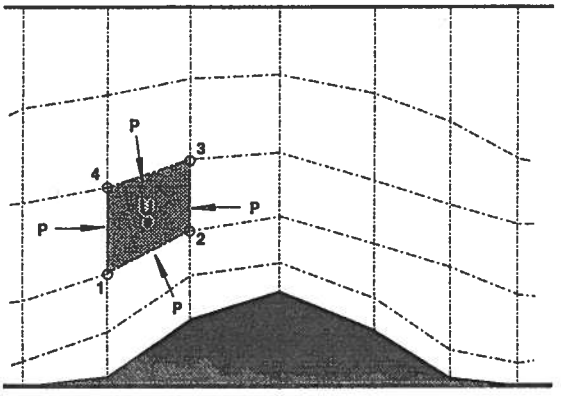

Figure 1. The finite-volume discretization in terrain-following coordinates.

third law states that 'to every action there is always opposed an equal reaction'. By the virtue of the finite-volume discretization (see Fig. 1), Newton's third law is automatically satisfied. Referring to Fig. 1, the contour integral can be further decomposed as follows:

$$\Sigma \mathbf{F}_x = -\left[\int_1^2 P \, \mathrm{d}z + \int_2^3 P \, \mathrm{d}z + \int_3^4 P \, \mathrm{d}z + \int_4^1 P \, \mathrm{d}z \right] \tag{3}$$

and

$$\Sigma \mathbf{F}_z = \int_1^2 P \, \mathrm{d}x + \int_3^4 P \, \mathrm{d}x \tag{4}$$

where points 1, 2, 3, and 4 are the four vertices of the finite volume.

The derivation so far is for the general non-hydrostatic flow. For a hydrostatic system, the following condition must hold

$$\Sigma \mathbf{F}_z = g \Delta m \tag{5}$$

where g is the acceleration due to gravity. Equation (5) states that the vertical component of the resultant pressure force acting on the finite volume exactly balances the total weight of the finite volume. The horizontal acceleration, after eliminating Δm from (2) using (5), can be written as

$$\frac{\mathrm{d}u}{\mathrm{d}t} = g \frac{\Sigma \mathbf{F}_x}{\Sigma \mathbf{F}_z} = g / \tan \gamma \tag{6}$$

where γ is the angle between the resultant pressure force and the horizontal surface. Equation (6) states that, for a hydrostatic system, the momentum acceleration due to the horizontal pressure gradient is simply the gravitational acceleration divided by the slope ($\tan \gamma$) of the resultant pressure force acting on the finite volume. The slope should never vanish if the hydrostatic approximation is valid. The process of eliminating Δm using (5), the exact hydrostatic balance equation for the finite volume, ensures the hydrostatic consistency of the algorithm.

Equation (6) is central to the finite-volume integration method, and it is exact for an arbitrary finite volume in a hydrostatic flow. To carry out the contour integration, assumptions regarding the subgrid distribution of the thermodynamic variables must be made. The accuracy of the method thus depends on how well the assumed subgrid distribution

approximates the true (unknown) distribution. This is analogous to the finite-volume discretization of the advective process in which the accuracy depends on the assumed subgrid distribution of the advected constituent (Lin *et al.* 1994; Lin and Rood 1996).

The simplest and physically meaningful approximation is the piecewise linear distribution. It turns out that the linear subgrid distribution assumption for the contour integration is sufficiently accurate (see numerical experiments in section 4), and it greatly simplifies the final algorithm. In the following development, it is assumed that P and ϕ (geopotential) are given at the four vertices of the finite volume, and that P is a linear function of ϕ between the vertices along the contour. This is an excellent approximation if the density gradients are small (e.g., the ocean). The contour integrals can be easily carried out under such a simplified assumption. As an example, the first term on the right hand side of (3) is approximated as

$$\int_1^2 P \, \mathrm{d}z \approx \frac{1}{2g}(P_1 + P_2)(\phi_2 - \phi_1).$$

Other integrals can be similarly carried out. After some cancellations, we obtain the following surprisingly simple form of the acceleration due to the pressure gradient force in the x-direction

$$\frac{\mathrm{d}u}{\mathrm{d}t} = \frac{(P_2 - P_4)(\phi_1 - \phi_3) + (P_1 - P_3)(\phi_4 - \phi_2)}{\Delta x[(P_2 - P_4) + (P_1 - P_3)]}. \tag{7}$$

Geopotential is computed by integrating vertically the hydrostatic relation $\dfrac{\partial \phi}{\partial P} = \dfrac{-1}{\rho}$ over one layer to obtain

$$\delta\phi = -\frac{1}{\rho_0}\delta P \tag{8}$$

where $\delta(\,)$ represents the vertical difference operator (between vertices), and ρ_0 is a suitably defined mean density between the vertices.

Geopotential computed by (8) is exact regardless of the density distribution if ρ_0 is the mean density in the *mean value theorem* sense. In the finite-difference sense, the mean density ρ_0 is said to be staggered vertically with respect to ϕ. Equation (7) together with Eq. (8) are best suited for flows in which density ρ is locally nearly a constant (e.g., the ocean). For constant density flow, the linear subgrid distribution is exact, and there will be no pressure gradient error. For flows with strong spatial density gradients the model resolution should be fine enough to adequately resolve the density variation. Clearly, a finite-volume advection scheme that predicts the volume mean density should be preferred for the discretization of the advection equation.

3. The finite-volume discretization in pressure-based terrain-following coordinates

Pressure-based vertical coordinates (e.g., sigma or hybrid sigma–P) are commonly adopted for modelling large-scale hydrostatic atmospheric flows in which the density variation in space, particularly in the vertical direction, is great. Different thermodynamic variable should therefore be chosen. The finite-volume mean acceleration due to the horizontal pressure gradient force can be derived by integrating analytically the pressure

gradient term in P-coordinate (here we have assumed the flow is hydrostatic) as follows:

$$\frac{du}{dt} = -\frac{\int\int \frac{\partial \phi}{\partial x}\, dx\, d\pi}{\int\int dx\, d\pi} \tag{9}$$

where π (to be specified later) is a monotonic function of P in the vertical direction. The volume integral in the denominator of (9) signifies the 'area' of the finite volume (the shaded area in Fig. 1). The volume integrals can be transformed into contour integrals using the *Green's theorem*. Equation (9) thus reduces to

$$\frac{du}{dt} = \frac{\int_C \phi\, d\pi}{\int_C \pi\, dx}. \tag{10}$$

Equation (10) is equivalent to (6). As in section 2, given values of ϕ and π at the four vertices, the contour integrals can be carried out by assuming, as in the previous section, the linear subgrid distribution. The resulting formula is

$$\frac{du}{dt} = \frac{(\pi_2 - \pi_4)(\phi_1 - \phi_3) + (\pi_1 - \pi_3)(\phi_4 - \phi_2)}{\Delta x[(\pi_2 - \pi_4) + (\pi_1 - \pi_3)]}. \tag{11}$$

Equation (11) is equivalent to (7). For a system in which the potential temperature (θ) is a prognostic variable, π is chosen to be P^κ, and the geopotential is computed as follows:

$$\delta\phi = -C_p\theta_0\delta P^\kappa \tag{12}$$

where C_p is the specific heat at constant pressure, R is the gas constant, $\kappa = R/C_p$, and θ_0 is the layer mean potential temperature.

If temperature (T) is a prognostic variable, $\pi = \ln(P)$, and the geopotential should be computed as follows:

$$\delta\phi = -RT_0\delta(\ln P) \tag{13}$$

where T_0 is the layer mean temperature. Analogous to the case presented in section 2, the layer mean θ_0 or T_0 is said to be staggered vertically with respect to ϕ.

Geopotential at the vertices of the finite volume is obtained by integrating (12) or (13) from the bottom surface to the model top layer-by-layer. This is different from the usual arrangement of the 'Lorenz grid' in which the geopotential, the horizontal momentum, and the potential temperature are defined at the same vertical level. The fact that the geopotential and the potential temperature in the Lorenz grid are defined at the same vertical level (e.g., in the Arakawa–Suarez method) mandates that in the computation of ϕ some sort of averaging of θ must be taken, which is the source of the vertical computational mode (see Fig. 2 in Arakawa and Kornor (1996) for a graphical illustration). The finite-volume integration method leads to a modified Lorenz grid in which the geopotential is staggered vertically with respect to the potential temperature and the horizontal momentum.

For an isentropic or an isothermal atmosphere, the true subgrid distribution of ϕ (as computed by (12) or (13)) is linear. Accordingly, the pressure gradient force computed by (11) is exact. It is obvious that Eq. (13) should not be used for computing the geopotential if the model top pressure is zero.

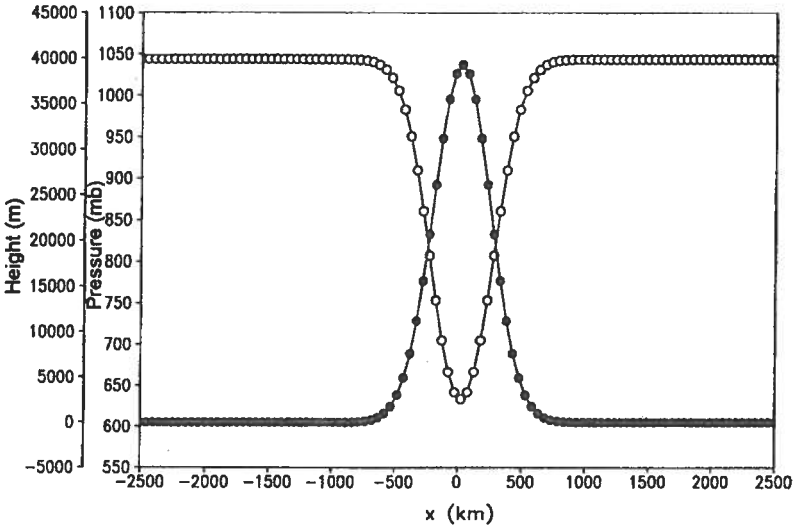

Figure 2. The mountain height (m) and the computed surface pressure (mb).

4. Numerical experiments

To evaluate the accuracy of the finite-volume integration method, two numerical experiments were devised. The first experiment is a static evaluation of the pressure gradient errors in a 2D vertical cross-section with a Gaussian mountain. The second experiment evaluates the dynamic response to the pressure gradient errors in a General Circulation Model environment. The Arakawa–Suarez method (their Eqs. 8.2–8.7) is chosen for the comparison. Similar numerical experiments have been used by several previous authors (e.g., Mesinger and Janjic 1984; Mihailovic and Janjic 1986) for evaluating the accuracy of various methods.

In the first experiment, the east–west domain is periodic ranging from $x = -X_{\max}$ to $x = X_{\max}$. The height of the mountain $H(x)$ is prescribed as follows:

$$H(x) = H_{\max} \mathrm{e}^{-(\frac{x}{D})^2}$$

where $H_{\max} = 4$ km and $D = X_{\max}/8$. The half-width of the domain $X_{\max}$ is chosen to be 2500 km. This is a moderately steep terrain. The atmosphere is at rest in hydrostatic equilibrium with a constant lapse-rate of 20/3 (K km^{-1}). The model top is located at 10.5 km (250 mb). The 'sea level' temperature is set to be 288 K. The temperature at the model top is therefore 218 K. The horizontal resolution is fixed at 50 km. To examine the convergence of these two methods, different vertical resolutions were used with equal spacing in the sigma coordinate. The Arakawa–Suarez method uses the potential temperature as the thermodynamic variable. Therefore, Eq. (11) together with (12) were used for direct comparison.

Given the constant lapse rate, the pressure and the geopotential at the edges of the sigma layers can be computed exactly by integrating the hydrostatic relation. The layer centred potential temperature can then be unambiguously determined using (12). Figure 2 shows the terrain and the computed surface pressure. Figure 3 shows the computed potential temperature contours.

The C-Grid staggering is utilized in the horizontal. Both the finite-volume method and the Arakawa–Suarez method generated errors in this constant-lapse-rate atmosphere.

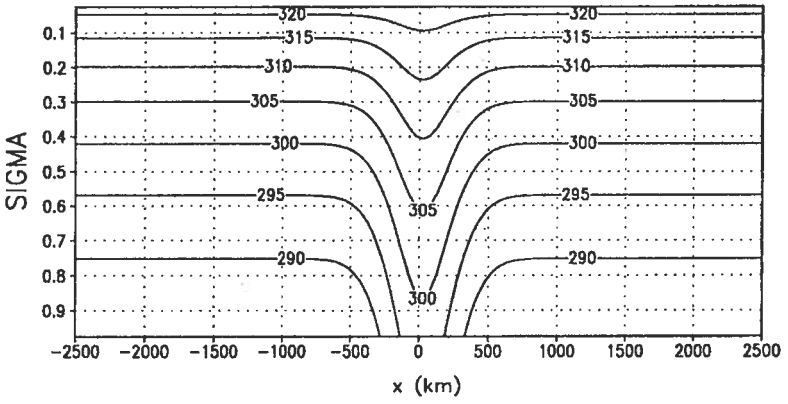

Figure 3. The computed potential temperature (K) in the constant-lapse-rate atmosphere.

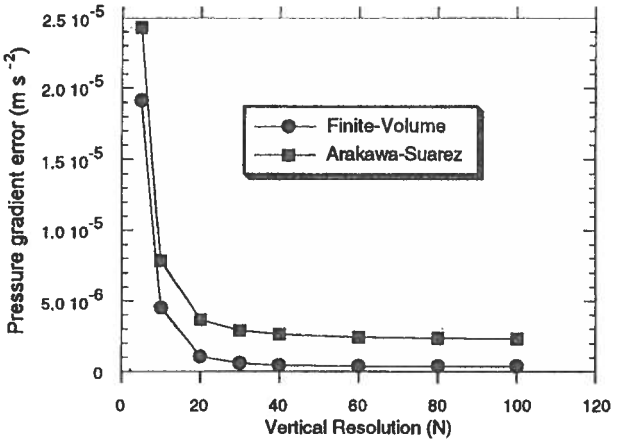

Figure 4. Mean absolute pressure gradient error (m s^{-2}) as a function of the total number of the vertical layers in the 2D domain.

Figure 4 shows the domain mean absolute errors as a function of the vertical resolution N, where N is the total number of layers. (The absolute error is defined as the absolute value of the computed pressure gradient.) The finite-volume method generated much smaller errors at all resolutions. In both methods, the errors reduce rapidly as N is increased from 5 to 20. The convergence rates decrease dramatically as N is further increased. The errors hardly decrease for N greater than 60, which is clearly due to the fixed horizontal resolution. To further reduce the error, it is clear that horizontal resolution must be consistently increased. The residue error in the finite-volume method after the 'convergence' is achieved (for N greater than 80) is substantially smaller than that of the Arakawa–Suarez method, suggesting that the proposed method is intrinsically more accurate.

The spatial distribution of the pressure gradient errors for $N = 20$ are shown in Fig. 5 and Fig. 6 for the Arakawa–Suarez method and the finite-volume method, respectively. The error in the finite-volume method is concentrated near the model top. This is because the linear subgrid distribution is a poorer approximation near the model top where the potential temperature has the highest gradient. A higher-order subgrid distribution should further reduce the error, particularly near the model top. The author has experimented

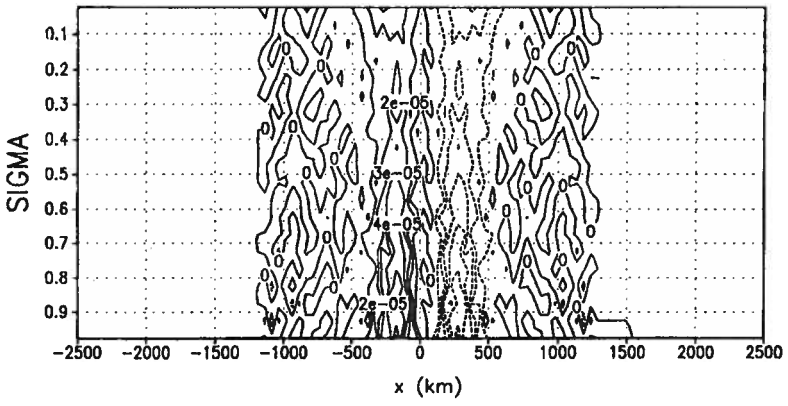

Figure 5. The pressure gradient (m s^{-2}) computed by the Arakawa–Suarez method. Contour interval is 1×10^{-5}.

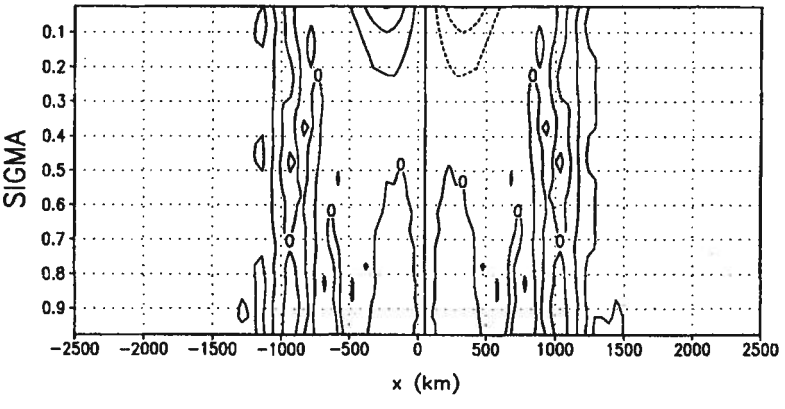

Figure 6. As in Fig. 5, but for the finite-volume method.

with some higher-order subgrid distributions. Preliminary results confirmed the above assertion. In contrast to the finite-volume method, the much larger error generated by the Arakawa–Suarez method is more uniformly distributed in the vertical.

Similar experiments using different horizontal resolution have also been carried out. The finite-volume method tends to perform increasingly better than the Arakawa–Suarez method at coarser horizontal resolution.

To evaluate the dynamic responses to the pressure gradient errors in a more realistic environment, the finite-volume method was implemented in a GCM framework and compared with the operational dynamical core for the Goddard Earth Observing System–General Circulation Model (GEOS–GCM). As remarked previously the finite-volume method for computing the pressure gradients works best if a finite-volume scheme is also used for the transport. A plug compatible 'dynamical core' for the GEOS–GCM based on the Flux-Form Semi-Lagrangian (FFSL) Scheme (a finite-volume method; see Lin and Rood 1996 and Lin and Rood 1997 for details) has been constructed (referred to as the FFSL core hereafter). The operational dynamical core for the GEOS–GCM (see Suarez and Takacs 1995 for details; S–T core hereafter) utilizes the Arakawa–Suarez method for the vertical advection of θ and the discretization of the pressure gradients. Table 1 lists the fundamentals of the two dynamical cores for the GEOS–GCM.

TABLE 1. FUNDAMENTALS OF THE GEOS–GCM DYNAMICAL CORES

Dynamical cores for GEOS–GCM	Operational core (Suarez and Takacs 1995)	Flux-form semi-Lagrangian core
Horizontal discretization	4th order extension of Arakawa and Lamb (1981)	Flux-form semi-Lagrangian (Lin and Rood 1997)
Vertical advection	Arakawa and Suarez (1983)	Finite-volume (3rd order for variable grid spacing)
Pressure gradients	Arakawa and Suarez (1983)	Finite-volume integration
Time integration	Leapfrog with Robert–Asselin filter	Explicit forward transport backward forcing
Subgrid mixing mechanism	16th order Shapiro filter	Monotonicity constraint

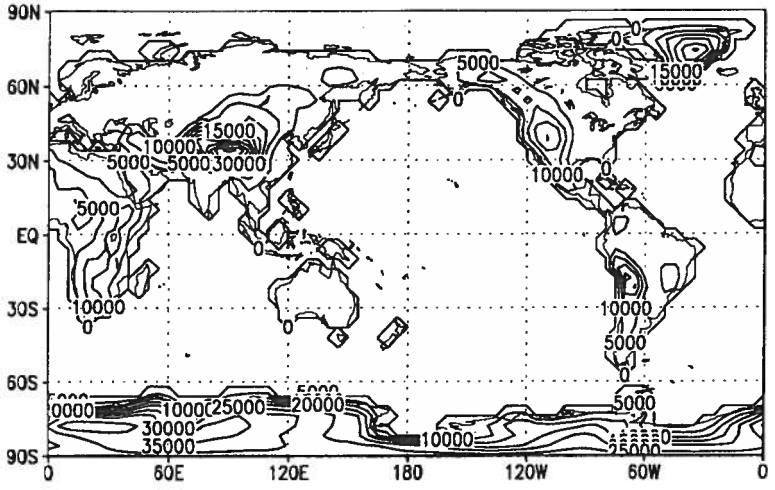

Figure 7. Topography contours.

The horizontal resolution is $4^\circ \times 5^\circ$ (latitude $\times$ longitude) and there are 20 unevenly spaced sigma layers in the vertical direction with the model top at 10 mb, which was the standard GEOS–GCM set up for long term climate integrations. The topography (Fig. 7) was generated from the US NAVY 10-minute dataset. These two dynamical cores were initialized with a resting atmosphere in hydrostatic equilibrium. The temperature profile is assumed to be a piecewise linear function of height (z), which is very similar to that of the US standard atmosphere. Below 10.5 km the temperature profile is the same as in the first experiment. There is an isothermal layer (218 K) between 10.5 km and 20 km. Above 20 km, the temperature increases at a constant lapse rate to 228 K at the model top at 31.25 km (10 mb). The initial surface pressure (see Fig. 8) and the potential temperature are computed in the same way as in the first example.

Since a motionless atmosphere in hydrostatic equilibrium should remain motionless, motions generated are considered as errors caused by the use of the sigma-coordinate. Both models were run for 5 days with time steps of 5 min and 10 min for the S–T core and the FFSL core, respectively. Figure 9 shows the global mean [error] kinetic energy generated by the FFSL core. The errors are extremely small and are plotted for both models in Fig. 10. After only a few days, the kinetic energy of the spurious motions generated by the S–T core is two orders of magnitude greater than that of the FFSL core. While the

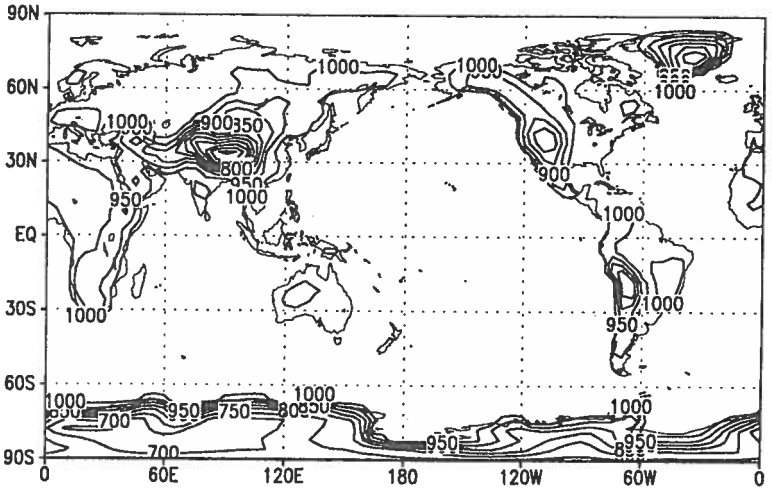

Figure 8. Initial surface pressure (mb).

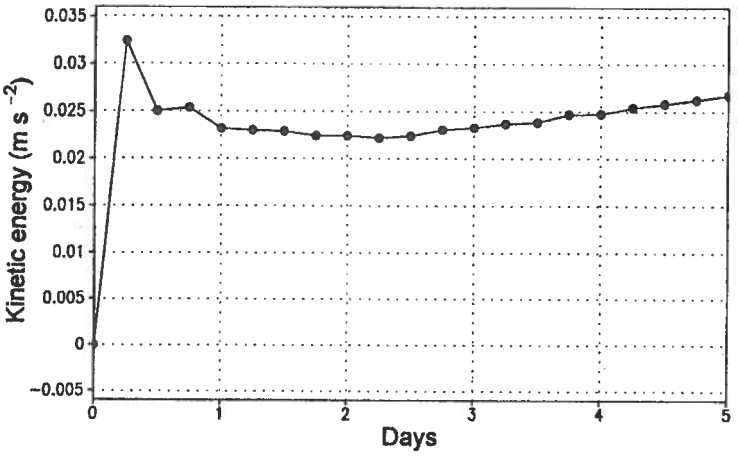

Figure 9. Global mean kinetic energy as a function of time (days) in the FFSL core.

spurious motion in the FFSL core is near equilibrium after six hours, the errors in the S–T core continue to grow beyond day 5 (not shown).

In the Arakawa–Suarez method the pressure gradient force is constrained to generate no circulation of vertically integrated momentum along a topography contour. It is thus anticipated that the vertically integrated circulation in the S–T core to be much reduced. The vertically integrated wind vectors at day 5 were plotted in Fig. 11 and Fig. 12 for the S–T core and the FFSL core, respectively. Note that the wind vectors in Fig. 12 were magnified 10 times (compared to Fig. 11) for visualization. After the expected cancellations, the vertically integrated wind errors in the S–T core are still more than an order of magnitude larger than that in the FFSL core. The (error) wind vectors in both models are concentrated near steep mountains.

The largest errors are located near the Himalayas. Figures 13 and 14 show the error kinetic energy in the vertical cross section at 30°N at day 5 for the S–T core and the FFSL

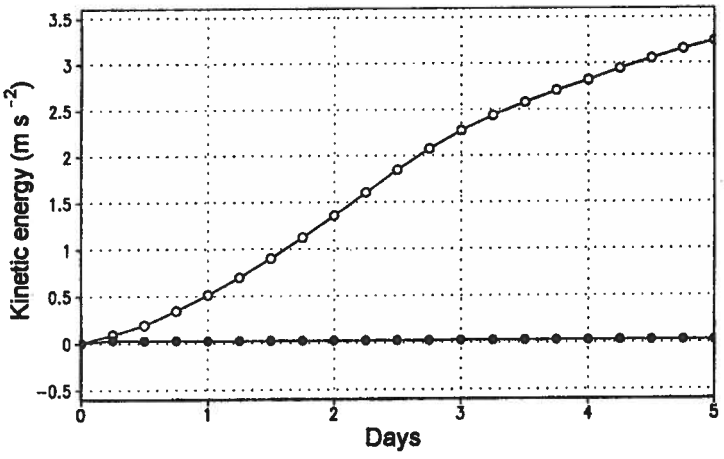

Figure 10. As in Fig. 9, but also for the S–T core (open circles).

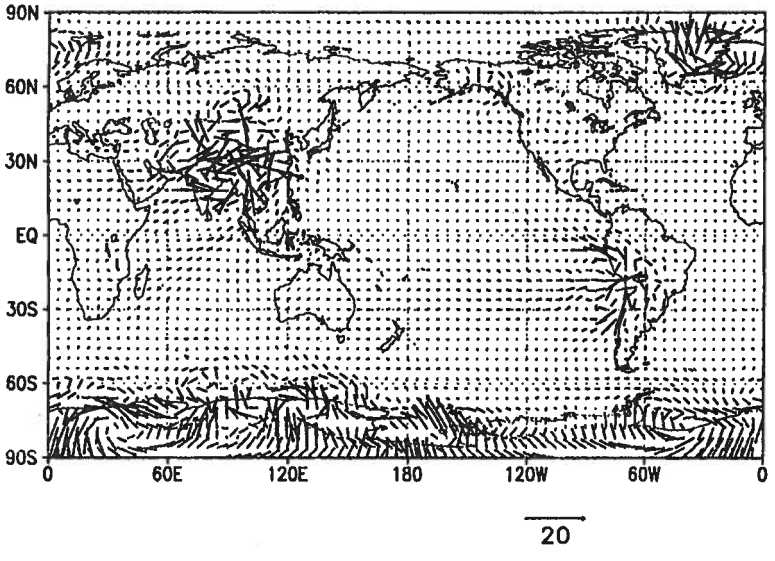

Figure 11. Vertically integrated winds generated in the S–T core.

core, respectively . (Note that different contour intervals are used.) In the S–T core, the errors are concentrated near the model's tropopause level. In the FFSL core, the errors are more concentrated near the model top (the top model layer has the largest error), as in the 2D case. This again is because the linear subgrid distribution approximation of ϕ becomes progressively worse as the model top is approached from below. Errors near the model top in the FFSL core can therefore be greatly reduced if a hybrid sigma–P coordinate is used.

5. Concluding remarks

A finite-volume integration method for computing the pressure gradient force in general vertical coordinates is described. The method is first derived for height based

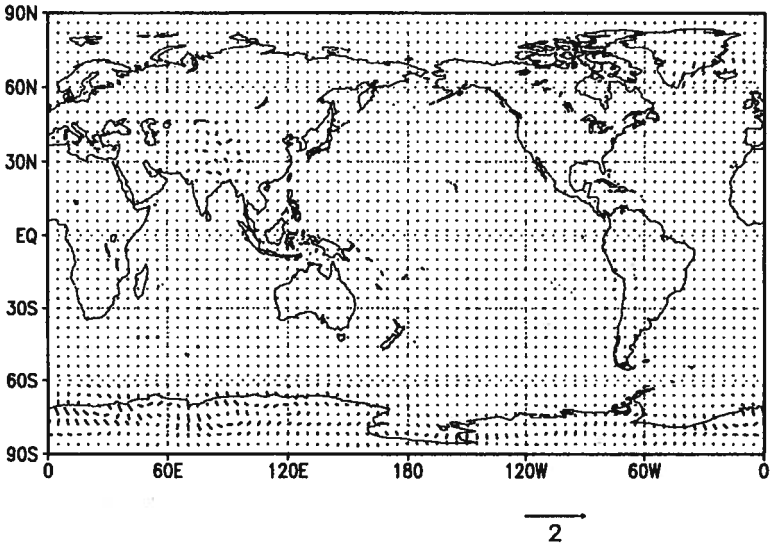

Figure 12. Vertically integrated winds generated in the FFSL core.

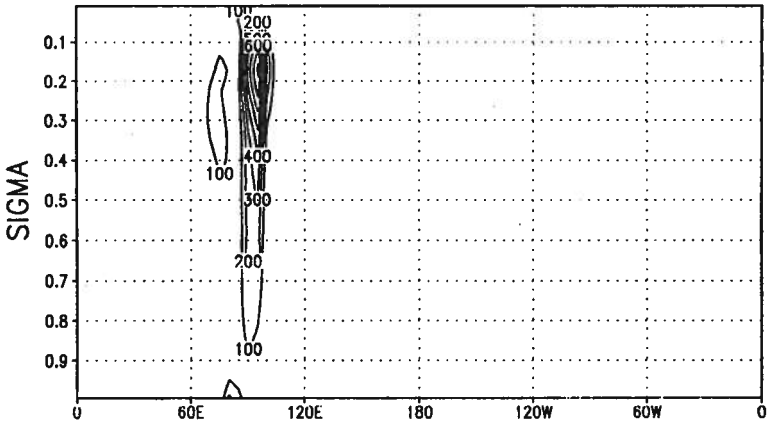

Figure 13. Error kinetic energy at 30 °N at day-5 in the S–T core. Contour interval = 100 m s^{-2}.

vertical coordinates using basic physical principles for the finite volume. An equivalent algorithm for pressure based vertical coordinates is then derived using the alternative method of integrating directly the pressure gradient term in the pressure coordinate for an arbitrary finite volume. The finite volume integration is carried out by first using the *Green's theorem* to transform the volume integrals into the contour integrals. To enable the contour integration, the subgrid distributions of P (the pressure) and ϕ (the geopotential) for the height-based and the pressure-based coordinates, respectively, were assumed to be linear along the contour. The resulting algorithm is compact, and it leads naturally to a modified Lorenz grid in which the geopotential is staggered vertically with the potential temperature.

The finite-volume integration method avoids the use of the analytic coordinate transformation for the pressure gradient terms, which is the main source of the inconsistencies

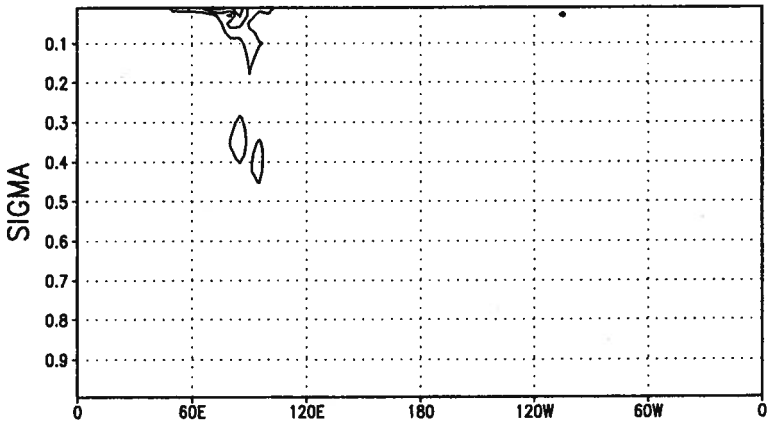

Figure 14. As in Fig. 13, but for the FFSL core. Contour interval = 2 m s^{-2}.

in many of the previously known methods. The vertical interpolation methods (e.g., Kurihara 1968; Mihailovic and Janjic 1986) also avoid the use of coordinate transformation. However, these methods do not, in general, satisfy Newton's second and the third laws since interpolation, rather than integration, was performed.

As the only approximation needed in the derivation of the finite-volume integration method is the subgrid distribution of P or ϕ, the accuracy of the method could be further improved by using a higher-order subgrid distribution for carrying out the contour integrations. For example, the quadratic subgrid distribution could be used. However, the resulting algorithm will not be as compact as (7) or (11). The linear subgrid distribution presented in this study is a good compromise between algorithm simplicity and accuracy. The author is currently exploring some of the higher-order extensions in an effort to find an optimal balance between algorithm complexity and accuracy. Nevertheless, as demonstrated in section 4, the current approach of using the linear subgrid distribution is sufficiently accurate.

As demonstrated in the 3D experiment, to receive the most benefit from using the finite-volume integration method, a finite-volume scheme that predicts the 'finite-volume' mean values should also be used for the advection of the chosen thermodynamic variable (density, potential temperature, or temperature). To reduce the concentrated error near the model top, a hybrid sigma–P or sigma–θ or a higher order subgrid distribution should be considered. Alternatively, more vertical levels can be placed at the region where large vertical potential temperature gradients exists.

6. Acknowledgements

Financial and computational support for this work is provided through the NASA Earth Observing System Program via the contract with the General Sciences Corp at NASA/GSFC. Dr R. B. Rood, head of the Data Assimilation Office, NASA/GSFC, provided the inspiration and moral support.

References

Arakawa, A. and Konor, C. S. 1996 Vertical differencing of the primitive equations based on the Charney–Phillips grid in hybrid σ–p vertical coordinates. *Mon. Weather Rev.*, **124**, 511–528

Arakawa, A. and Lamb, V. R.	1981	A potential enstrophy and energy conserving scheme for the shallow water equations. *Mon. Weather Rev.*, **109,** 18–36
Arakawa, A. and Suarez,M. J.	1983	Vertical differencing of the primitive equations in sigma coordinates. *Mon. Weather Rev.*, **111,** 34–45
Corby, G. A., Gilchrist, A. and Newson, R. L.	1972	A general circulation model of the atmosphere suitable for long period integrations. *Q. J. R. Meteorol. Soc.*, **98,** 809–832
Gal-Chen, T. and Somerville, R. C. J.	1975	On the use of a coordinate transformation for the solution of the Navier–Stokes equations. *J. Comput. Phys.*, **17,** 209–228
Kasahara, A.	1974	Various vertical coordinate systems used for numerical weather predictions. *Mon. Weather Rev.*, **102,** 509–522
Lin, S.-J., Chao, W. C., Sud, Y. C. and Walker, G. K.	1994	A class of the van Leer-type transport schemes and its applications to the moisture transport in a general circulation model. *Mon. Weather Rev.*, **122,** 1575–1593
Lin, S.-J. and Rood, R. B.	1996	Multidimensional flux-form semi-Lagrangian transport schemes. *Mon. Weather Rev.*, **124,** 2046–2070
	1997	An explicit flux-form semi-Lagrangian shallow water model on the sphere. *Q. J. R. Meteorol. Soc.* in press
Mesinger, F.	1994	A blocking technique for representation of mountains in atmospheric models. *Rev. Meteorol. Aeronaut.*, **44,** 195–202
Mesinger, F. and Janjic, Z. I.	1984	'Finite-difference schemes for the pressure gradient force and for the hydrostatic equation'. Pp. 103–157 in Proceedings of the 1983 ECMWF seminar on numerical methods for weather prediction. European Centre for Medium Range Weather Forecasts, Shinfield Park, Reading, UK
Mihailovic, D. T. and Janjic, Z. I.	1986	Comparison of methods for reducing the error of the pressure gradient force in sigma coordinate models. *Meteorol. Atmos. Phys.*, **35,** 177–184
Phillips, N. A.	1957	A coordinate system having special advantage for numerical forecasting. *J. Meteorol. Soc.*, **14,** 184–185
Simmons, A. J. and Burridge, D. M.	1981	An energy and angular-momentum conserving vertical finite-difference scheme and hybrid vertical coordinates. *Mon. Weather Rev.*, **109,** 758–766
Smagorinsky, J., Strickler, R. F., Sangster, W. E., Manabe, S., Holloway, Jr., J. L. and Hembree, G. D.	1967	'Prediction experiments with a general circulation model'. Pp. 70–134 in Proc. Int. Symp. on dynamics of large scale atmospheric processes. Moscow, 23–30 June 1965, Izdatel'sstvo Nauka, Moscow
Stelling, G. S. and Van Kester, J. A. Th. M.	1994	On the approximation of horizontal gradients in sigma co-ordinates for bathymetry with steep bottom slopes. *International Journal for Numerical Methods in Fluids*, **18,** 915–935
Suarez, M. J. and Takacs, L. L.	1995	Documentation of the ARIES/GEOS dynamical core: Version 2. *NASA Technical Memorandum* 104 606, Vol. 5